

# Overcoming the Zero-Rate Hashing Bound with Holographic Quantum Error Correction

J. Fan<sup>1,2\*</sup>, M. Steinberg<sup>1,2\*</sup>, A. Jahn<sup>3</sup>, C. Cao<sup>4</sup>, S. Feld<sup>1,2</sup>

<sup>1</sup>*QuTech, Delft University of Technology, 2628 CJ Delft, The Netherlands*

<sup>2</sup>*Quantum and Computer Engineering Department, Delft University of Technology, 2628 CD Delft, The Netherlands*

<sup>3</sup>*Department of Physics, Freie Universität Berlin, 14195 Berlin, Germany and*

<sup>4</sup>*Department of Physics, Virginia Tech, Blacksburg, VA 24061, USA*

Several recent techniques for modifying topological codes with single-qubit Clifford operators have shown high resilience against pure Pauli noise. Paramount to these findings has been the demonstration that several variants exhibit error thresholds often attaining or exceeding the zero-rate hashing bound, a known benchmark for code-capacity noise channels, for biased noise. Additionally, direct comparison with the hashing bound has shown that several topological codes outperform the hashing bound at points of finite Pauli noise biases. Motivated by these observations, we study zero-rate holographic quantum error correction codes, discovering very high threshold values under diverse and finitely-biased noise channels using a tensor-network decoding approach. Our results establish that all codes tested achieve or surpass the hashing bound at various points, ranging from pure 2-Pauli noise ( $\eta = 0$ ) to pure 1-Pauli noise ( $\eta = +\infty$ ), thereby demonstrating that holographic codes exhibit excellent error tolerance in the code-capacity picture. Such findings imply the existence of a structured and systematic method for constructing high-threshold codes suitable for realistically motivated noise channels. To our knowledge, this work is also the first instance of such remarkable threshold behavior in stabilizer quantum codes for the pure 2-Pauli noise regime, as well as for finitely-biased noise channels.

## I. INTRODUCTION

Utilizing principles from quantum error correction (QEC) is thus far the most viable path towards the construction of a large-scale, fault-tolerant quantum computer [1–3]. In the field of QEC, *stabilizer codes* [4] as well as *topological quantum codes* [5] have come to dominate the domain, of which ever more complex instances are being realized in experimental demonstrations [6–8]. In order to inform these experiments, simulations of error thresholds for entire classes of stabilizer codes have been implemented; here, the family of *surface codes* has become particularly prominent, due in large part to robust error thresholds under various error models of progressively more realistic circumstances, as well as their known practical appeal from local stabilizer checks and planar architectural layout [5, 9]. On the one hand, it is known that simple noise channels such as the quantum *erasure* and *depolarizing* channels do give preliminary information on how resilient a quantum code may be at the theoretical level [10, 11]. However, in practice, the experimental calculus is much different, with noise often biased towards a certain subset of Pauli errors, such as finitely-biased or pure  $Z$  noise found in qubit technologies which experience *dephasing* noise [6, 12–16], or a combination of several Pauli errors at once, as in the *square-lattice Gottesman-Kitaev-Preskill* (GKP) code [17–20]. It is in this area that topological codes (e.g. Clifford-deformed topological codes such as the *XZZX surface code*), concatenated codes based on repetition codes, as well as *graph states* yield exceptionally high thresholds for pure 1-Pauli  $X$ ,  $Y$ , or  $Z$  noise, achieving 50% in many cases [21–28]. In these studies, the assumptions necessary for biased-noise code-capacity explorations traditionally include independent and identically distributed (IID)

single-qubit Pauli channels

$$\mathcal{E}(\rho) = (1 - p)\rho + p(r_X X\rho X + r_Y Y\rho Y + r_Z Z\rho Z), \quad (1)$$

with the relative error probabilities  $r_X + r_Y + r_Z = 1$ , typically in the regime of  $r_X = r_Y$  with a bias  $\eta = \frac{r_Z}{r_X + r_Y} \geq \frac{1}{2}$  (in the case of  $Z$ -biased noise). When  $\eta = \frac{1}{2}$  one recovers the standard depolarizing noise channel. Additionally, the behavior of these  $Z$ -biased thresholds was studied, and it was found that such surface-code variants in many cases either match or exceed the error threshold bounds predicted by the zero-rate *hashing bound* [11].

In this work, we demonstrate that such intriguing behavior is also present in *holographic quantum codes* [29–33]. Using the tensor-network decoder described in [31, 34], we study the biased-noise error thresholds in detail for several zero-rate holographic codes. Such codes are derived from elemental *seed tensors* describing a simple code, contracted in a tensor network with hyperbolic geometry (Fig. 1). Here we test the *Harlow-Preskill-Pastawski-Yoshida* (HaPPY) model [29], whose seed tensor corresponds to the  $[[5, 1, 3]]$  code. We additionally test: the Steane code [32]; the  $[[6, 1, 3]]$  code [31]; and the holographic *surface-code fragment* (SCF) [30]. For all of the codes tested, we find evidence of highly resilient code-capacity thresholds and display characteristics of their resulting ternary biased-noise plots. Key results in our work include: 1) Evidence that the zero-rate HaPPY code exhibits 50% error thresholds for pure biased Pauli noise. 2) The holographic Steane code obtains a depolarizing noise threshold of 18.985%, competitive with known code-capacity bounds derived for several topological codes using a mapping to statistical-mechanical models [35]; 3) For several pure 2-Pauli noise channels (i.e., consisting of a subset of two out of the three Pauli errors), the zero-rate SCF and  $[[6, 1, 3]]$  holographic codes exceed current state-of-the-art results [28, 36], in addition to surpassing the hashing bound. 4) Finally, for all of the codes evaluated, error thresholds were found to overtake the bound for numerous finitely-biased points on the hashing

\* These authors contributed equally to this work.

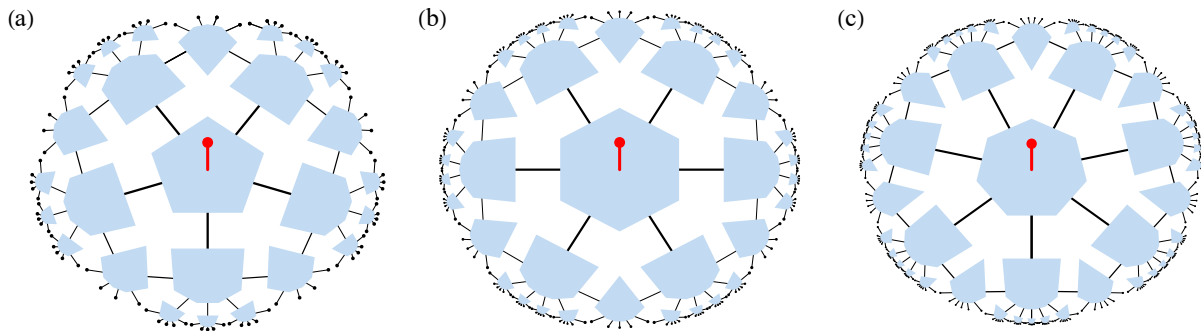


FIG. 1. The holographic tensor-network codes considered in this work: (a) The *Harlow-Preskill-Pastawski-Yoshida* (HaPPY) code [29] whose pentagon-hexagon geometry also underlies the holographic *surface-code fragment* (SCF) model [30], (b) the holographic  $[[6, 1, 3]]$  code [31], and (c) the holographic Steane code [32]. All are defined as tensor network contractions of copies of a fixed  $q$ -leg tensor on a hyperbolic tiling, with the central tensor used as a *seed tensor* for the encoding isometry of a  $[[q - 1, 1, d]]$  code with some distance  $d$ . The remaining tensors have all  $q$  legs contracted in the plane, leading to a larger encoding map between one logical qubit (central red leg) and the boundary physical qubits (open black legs). Here we depict the codes with  $L = 2$  layers of edge inflation. In the  $L \rightarrow \infty$  limit, the rate of each code goes to zero.

curve, within the bias range of  $0 \leq \eta \leq +\infty$ . Our results strongly suggest that holographic quantum codes possess high resilience against various types of noise, bolstering the case that these codes may find utility in practical quantum information processing.

## II. HOLOGRAPHIC QUANTUM ERROR CORRECTION

Holographic quantum codes at their core are *subsystem stabilizer* codes [4, 37, 38]. Stabilizer codes themselves are defined as codes for which the *logical operators*  $\mathcal{L}$  and *code-word stabilizers*  $\mathcal{S}$  consist of elements  $P_i \in \mathcal{P}^n$ , where  $\mathcal{P}^n$  is the  $n$ -qubit Pauli group,  $P_i$  takes the form  $P_{i_1} \otimes \cdots \otimes P_{i_n}$ , and  $P \in \{I, X, Y, Z\}$ , i.e., the single-qubit Pauli operators. In subsystem stabilizer codes such as holographic codes, one typically can choose to subdivide the physical Hilbert space as  $\mathcal{H}_p = \mathcal{H} \otimes \bar{\mathcal{H}}$ , where  $\mathcal{H}$  represents the code subspace. It is also given that  $\mathcal{H}$  can be decomposed as  $\mathcal{H} = \mathcal{H}_L \otimes \mathcal{H}_G$ , where  $\mathcal{H}_L$  and  $\mathcal{H}_G$  represent the *logical* and *gauge* subsystems of the code subspace, respectively; holographic codes were first treated as such subsystem stabilizer codes in [38–40]. In this work, however, we consider only zero-rate versions of holographic codes, wherein only the central logical index remains (Figure 1). Additionally, we mention here that it is possible to construct *non-Abelian stabilizer*, *non-stabilizer*, or even *approximate* quantum codes in the holographic context [39, 41–44]; however, we shall limit ourselves to stabilizer versions of holographic quantum codes in the present work.

Originally developed to model the *AdS/CFT correspondence* [45–49], holographic quantum error correction involves encoding maps from *bulk* (logical) degrees of freedom on a  $d+1$ -dimensional hyperbolic space to  $d$ -dimensional *boundary* (physical) degrees of freedom. While in full AdS/CFT the bulk and boundary degrees of freedom are associated with weakly-coupled quantum gravity on an asymptotically anti-de Sitter (AdS) background and strongly-coupled conformal field theory (CFT), respectively, aspects of this duality for  $d = 1$  can be captured by simple tensor network

codes [29, 33, 50, 51]. From a practical perspective, there are many reasons to find the concept of a holographic quantum code appealing. Firstly, holographic codes are relatively simple to construct and scale from small, atomized examples to larger example codes. As a direct consequence of the quantum LEGO formalism [52], concepts such as code structure and transversal logical operations are straightforward to intuit. Secondly, the boundary of holographic codes exhibits a quasiperiodic self-similarity [53, 54], allowing one to rescale the number of physical and logical qubits using local *inflation rules* that also determine the code’s rate and distance scaling [34, 55]. Thirdly, encoding rates of holographic codes are known to be quite high and tunable [34], competitive with many recent proposals of quantum *low-density parity-check* (qLDPC) codes [56]. Fourthly, it is known that most seed tensors for holographic codes can be easily mapped to graph states, implying that efficient preparation schemes likely exist [57–60]. Lastly, and perhaps most consequentially, it has been shown that holographic codes exhibit high resilience against various noise channels. Indeed, it was first shown in [29] that holographic quantum error correction codes exhibit high thresholds against the quantum erasure channel; subsequently, several works have shown the capability of certain code constructions to protect against depolarizing and 1-Pauli noise, potentially as well as topological codes [30–32, 34, 55, 61]. However, to our knowledge, a systematic biased-noise threshold study for even zero-rate holographic codes has not been performed, let alone for their constant-rate versions<sup>2</sup>. As such, our work takes the first step towards understanding holographic codes under more generalized noise channels.

The main ingredient of a holographic quantum code is the seed tensor defining the encoding map for a single tile. Here we consider the zero-rate case with a logical qubit only on the central tile; on the remaining tiles all tensor legs are planar, effectively dispersing the logical information towards the tiling

<sup>2</sup> [62] discusses biased noise in finite-rate HaPPY pentagon codes, but it only captures the non-detectable error probability for a code of fixed length.

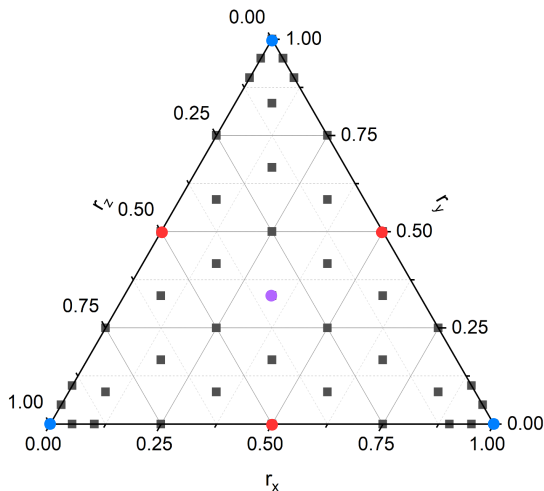


FIG. 2. Threshold data points surveyed for the holographic codes tested in this work. All data points were ascertained using four threshold crossing points at each corresponding marker in the diagram. In blue, we highlight the pure Pauli biased points, and in red, we have accentuated the 2-Pauli bias points considered in this work. The depolarizing noise point is denoted in violet.

boundary. Note that in generic holographic codes, each tile may hold a logical qubit, leading to a nonzero asymptotic rate as the number  $L$  of layers is increased. While copies of the same seed tensor are typically used in this case, one may also employ several different seed tensors [63] in a spirit similar to *heterogeneous* concatenation methods for tree-style concatenated codes [64, 65]. In Appendix A, we provide a table with all of the relevant information about each seed tensor for each code utilized in this work.

### III. RESULTS

Threshold calculations were performed using the tensor-network decoder from [31, 34]. These decoders and others will be made public in an upcoming software package for holographic quantum error correction codes [66]. However, for the purposes of understanding the current work, we focus on surveying biased-noise resilience for a swath of known holographic codes, and not on a systematic treatment of the tensor-network decoding methodology [67].

In our biased-noise threshold profiling, we tested 43 distinct Pauli biases and have displayed them on the ternary diagram shown in Figure 2. Each point of the triangular plot shown represents a pure Pauli error channel. Subsequently, points on the interior of the plot can be read by following the grid lines provided to the boundaries; for example, the point to the lower left of the central depolarizing noise marker can be interpreted as having relative biases  $\bar{r} = (r_X, r_Y, r_Z)$  of  $(0.25, 0.25, 0.5)$ . At each bias point 10,000 Monte Carlo simulations were performed per threshold curve data point, per layer. We display commensurate threshold curve results for some select data points in Appendix B for the zero-rate

HaPPY code.

The ternary plots for all four zero-rate holographic codes tested in this paper are depicted in Figure 3. From (a)-(d), we have displayed the: HaPPY; Steane;  $[[6, 1, 3]]$ ; and SCF. At the center of each diagram, where depolarizing noise is represented, the zero-rate HaPPY code exhibits the lowest resilience ( $p_{th} = 17.9\%$ ), whereas all other codes tested indicating thresholds in the region between  $p_{th} = 18\% \sim 19\%$ . As we move along each plot towards a pure 1-Pauli bias, we see starkly distinct behavior for every holographic code assessed: for example, the zero-rate HaPPY code (a) attains clear 50% thresholds in each of the pure 1-Pauli biases, while the Steane code's resilience (b) appears to decrease. In the  $[[6, 1, 3]]$  and SCF codes, we observe asymmetrical biased-noise profiles with respect to pure Pauli noise behavior. For the  $[[6, 1, 3]]$  code, we note that under pure 1-Pauli  $X$  and  $Y$  noise channels, the threshold of the code increases, albeit more slowly than for the HaPPY code; notwithstanding this similarity, the  $[[6, 1, 3]]$  code's threshold dips by a small amount as we move towards the pure- $Z$  region of the ternary plot. Interestingly, the SCF also evinces an asymmetrical biased-noise threshold spectrum. However, the SCF manifests high tolerance to pure  $Y$  errors, but to pure  $X$  and  $Z$  errors decreases, as in the Steane code.

If we look beyond the pure 1-Pauli portion of the ternary plots, we note more subtle behavior of these codes: for example, it can be seen that modest threshold increases emerge for the Steane and  $[[6, 1, 3]]$  codes as we move towards pure 2-Pauli noise, i.e.,  $XY$ ,  $YZ$ , and  $XZ$  noise. These changes can be seen more clearly by examining the threshold behavior of the codes by tuning a bias parameter  $\eta$ . In previous work, this aim was accomplished by comparing various zero-rate codes against the *hashing bound*, a useful lower bound for quantifying code-capacity channel performance [26]. However, in contrast to the present work, all previous works have examined the pure 1-Pauli noise limit associated with the hashing bound, and have not delved into combinations of two types of Pauli errors at once, a condition known to occur in the square-lattice GKP code under a symmetric Gaussian random displacement noise channel [17–20]. As such, we tune the  $\eta$  parameter within the range  $0 \leq \eta \leq +\infty$ , extending previous work past the regime indicated by  $\eta \geq 0.5$  [21, 25, 26]. The hashing bound is formally defined as

$$R = 1 - H(\bar{p}), \quad (2)$$

where  $R$  represents an achievable rate  $k/n$  for a random stabilizer code and  $H(\bar{p})$  represents the *Shannon entropy* [10, 11]

$$H(\bar{p}) = - \sum_{i \in \{X, Y, Z\}} p_i \log p_i. \quad (3)$$

Here,  $\bar{p} = p \bar{r}$ ,  $r_X + r_Y + r_Z = 1$  as stated before, and  $p$  represents the overall physical error probability. For a given noise model, there exists a physical error probability  $p$ , at some given relative bias vector  $\bar{r}$ , for which the achievable rate  $R$  goes to zero. This achievable rate via random coding is known as the *zero-rate hashing bound*.

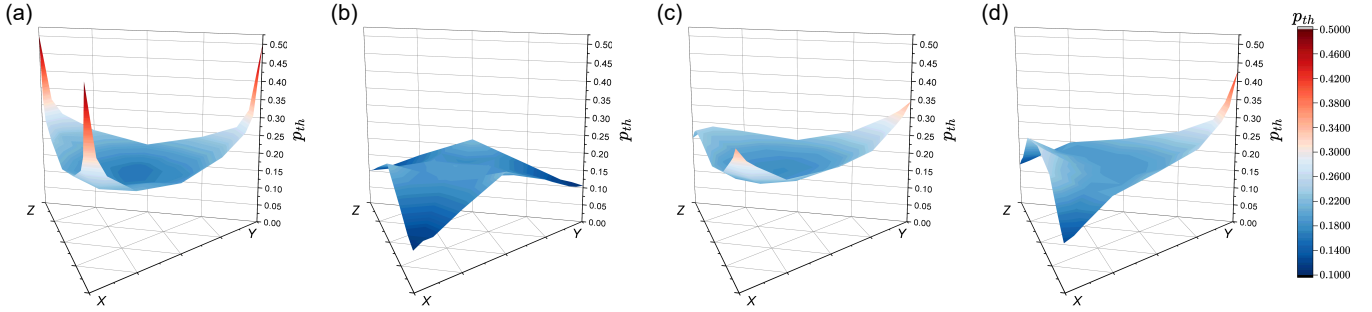


FIG. 3. Ternary plots for all holographic codes investigated in this study under biased noise, in the code-capacity setting. (a)-(d) depicts the zero-rate HaPPY, Steane,  $[[6, 1, 3]]$ , and SCF codes; thresholds are color-coded from dark blue ( $p_{th} = 10\%$ ) to dark red ( $p_{th} = 50\%$ ). Additionally, we tested the *tailored*  $[[7, 1, 3]]$  code from [25, 68], which achieved an identical threshold profile to that of the HaPPY code.

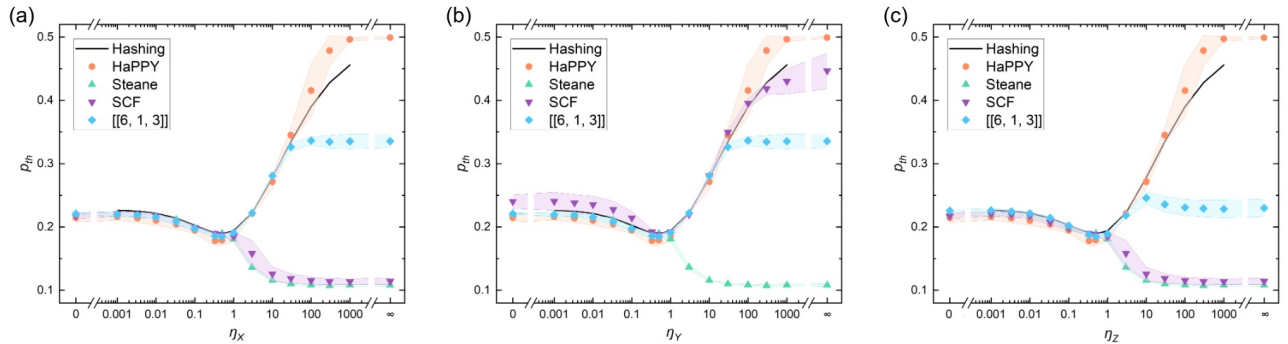


FIG. 4. Hashing bound plots for all of the codes tested in this work; we denote the hashing bound values in black solid line, while holographic codes are shown in varying colors and markers, together with calculated uncertainties. For all of the plots, biases ranged from  $\eta = \{0, +\infty\}$ . We list particular points of interest in Table I.

Figure 4 depicts the comparison of the zero-rate hashing bound for  $0 \leq \eta \leq +\infty$  with all four of the surveyed zero-rate holographic codes. In our plots, we calculate physical recovery rates for the following noise biases:

$$\eta \in (0, 1/1000, 33/10000, 99/10000, 33/1000, 1/10, 1/3, 1/2, 1, 3, 10, 30, 100, 300, 1000, +\infty). \quad (4)$$

In these results, the biased-noise properties of these codes manifest themselves across the full landscape of possible pure and 2-Pauli biases, i.e. pure  $X$ ,  $Y$ , and  $Z$  noise, in addition to pure  $XY$ ,  $YZ$ , and  $XZ$  noise. In (a)-(c), we illustrate the bias tuning for pure  $X$ ,  $Y$ , and  $Z$  biases; consequently, as we tune the parameter  $\eta$  in the direction towards zero, we effectively remove  $X$ ,  $Y$ , and  $Z$  noise from the simulations, in effect achieving, as  $\eta \rightarrow 0$ , pure  $YZ$  noise from (a), pure  $XZ$  noise from (b), and pure  $XY$  noise from (c). Table I displays several specific threshold points of interest in the ternary plots from Figure 3. Noise biases and their corresponding bias vectors are displayed, and figures in green and gold signify threshold data which either attain or exceed the hashing bound, or come with 2% of achieving the bound, respectively. As is evidenced in each of the plots, the zero-rate HaPPY code clearly achieves the hashing bound for all pure 1-Pauli biases, as well as for finite biases in which  $\eta > 10$ . Additionally, in the lim-

its for which  $\eta \rightarrow 0$ , the HaPPY code thresholds closely trace out the hashing bound as pure 2-Pauli noise is approached. Generally, the behavior of the HaPPY code emulates in large part the behavior seen of the *generalized toric code* family [25]. The Steane code portrays a distinct trend: in the pure 1-Pauli noise limit, the code performs significantly worse than all other codes tested. Nonetheless, the zero-rate Steane code eclipses the hashing bound for depolarizing noise ( $\eta = 0.5$ ), while also approaching the bound for finite biases as we approach the pure 2-Pauli limit ( $\eta = 0$ ). It was shown in previous work [24] that the color code exhibits similar behavior in the pure 1-Pauli bias regime; as such, it is logical to infer that the holographic Steane code manifests similar behavior in these limits. Due to the fact that both codes are built from self-dual CSS codes [37], in the 1-Pauli limit, only one set of stabilizers gives information about the error, while the other stabilizers do not yield additional information for decoding. As such, the problem reduces to a classical linear code with a check matrix defined by only half of the symplectic check matrix in the quantum code. Notwithstanding, it is known that many code concatenation schemes based on graph states can slightly exceed the hashing bound; our results, up to the uncertainty margin given, show that the holographic Steane can at least match most of the codes discovered in [28].

Noise Bias ( $r_X, r_Y, r_Z$ )	Hashing (%)	HaPPY (%)	Steane (%)	SCF (%)	[[6, 1, 3]] (%)
Depolarizing (1/3, 1/3, 1/3)	18.929	17.9 ± 0.81	18.98 ± 0.36	18.83 ± 0.13	18.46 ± 0.36
Pure X (1, 0, 0)	50.00	49.92 ± 0.096	10.79 ± 0.18	11.42 ± 0.52	33.56 ± 1.08
Pure Y (0, 1, 0)	50.00	49.91 ± 0.11	10.8 ± 0.19	44.66 ± 2.82	33.56 ± 1.08
Pure Z (0, 0, 1)	50.00	49.91 ± 0.11	10.8 ± 0.19	11.42 ± 0.52	22.99 ± 1.39
Pure XZ (1/2, 0, 1/2)	22.709	21.45 ± 0.68	22.1 ± 0.16	24.027 ± 1.08	22.08 ± 0.04
Pure XY (1/2, 1/2, 0)	22.709	21.45 ± 0.69	22.1 ± 0.17	21.77 ± 0.51	22.58 ± 0.17
Pure YZ (0, 1/2, 1/2)	22.709	21.45 ± 0.68	22.1 ± 0.17	21.77 ± 0.51	22.08 ± 0.04

TABLE I. Recovery threshold data points  $p_{th}$  for select pure and 2-Pauli biases. The entry in blue surpasses the hashing bound; entries in green attain it up to statistical uncertainty, while entries in gold come within 2% of achieving the bound.

The SCF displays very interesting behavior at several points in Figure 4. For biased  $X$  and  $Z$  noise, the SCF performs similarly to the Steane code as  $\eta \rightarrow +\infty$ ; this is due to the CSS properties of the seed tensor for both codes, as fewer parity checks are used for distinguishing errors in the limit of pure 1-Pauli noise. For biased  $Y$  noise, however, the SCF exhibits excellent threshold performance; although the SCF does not attain the hashing bound in the pure  $Y$  noise limit, many points of finite bias reach the bound. Additionally, as we tune the parameter  $\eta$  back towards zero, the pure  $XZ$  limit shows that the SCF surpasses the hashing bound at finite bias ( $\eta \leq 0.1$ ). To the best of our knowledge, no other code construction thus far has surpassed the hashing bound for 2-Pauli noise [28, 36].

Lastly, the [[6, 1, 3]] code also exhibits breakaway threshold behavior, albeit for pure  $XY$  noise. However, it can be observed in Figure 4 that various points within the finitely-biased range  $\eta \in [0, 0.5]$  come either within 2% of the hashing bound, or slightly exceeds it.

#### IV. CONCLUSION

In this work we have shown strong evidence of extremely high threshold behavior for zero-rate holographic quantum codes in the presence of 1-Pauli and 2-Pauli noise channels, for pure and finitely-biased noise regimes. In doing so, we have tested the HaPPY; Steane; [[6, 1, 3]]; and SCF codes, finding that all of them admit threshold points for some Pauli noise bias which either attain or surpass the hashing bound. In addition to these codes, the “tailored” [[7, 1, 3]] code from [68] was also tested; we found that the biased-noise ternary plot is identical to that of the HaPPY code. This result is in line with the conclusions from [25], which constructed generalized toric codes with performance surpassing the hashing bound in the pure 1-Pauli limit. In related work [55], an integer-optimization decoder was utilized for the zero-rate *Evenbly* code in order to pinpoint the depolarizing and pure 1-Pauli thresholds of 19.1% and 50%, respectively. It would be interesting to see if a tensor-network decoder would allow for such complete biased-noise threshold explorations of Evenbly codes [69–71]. Our work demonstrates that holographic

codes exhibit remarkable code-capacity properties under biased noise channels and can even overtake current state-of-the-art results [28]. It further indicates that they constitute a novel and competitive class of stabilizer codes that is robust against biased noise beyond the conventional options of topological codes [21–24, 26, 27], naïve constructions of concatenated codes, or graph codes [28]. These results affirm that holographic quantum codes could have practical utility for quantum computing. Taking stock of our results and in combination with recent work showing that the bulk geometric transition in AdS/CFT implies a threshold for holographic codes in the continuum limit [61], it is natural to ask whether the *discretized* isometric map typical of holographic codes provides a general method for constructing codes which faithfully achieve various finite points of the hashing bound. We leave this direction for future work. In the interests of practical quantum computing, one application of holographic quantum codes may be found in *magic-state distillation* [72, 73]. Indeed, for the case of the HaPPY and holographic Steane codes, the transversal logical  $\overline{SH}$  and  $\overline{H}$  gates allow for current state-of-the-art methods to be leveraged, as was pointed out in [74]. Also, as the holographic map can be applied to *XP-stabilizer codes* [44, 75], we additionally expect that further examples of holographic quantum codes can be constructed and examined. As a final note, we have only tested the zero-rate versions of many holographic codes, but one may test constant-rate holographic codes as well, as shown in [34]; the construction and testing of such codes is the subject of active research.

*Acknowledgements.* — We thank Aritra Sarkar, David Elkouss, and Jens Eisert for discussions related to concatenated codes, universal logical gate sets, as well as quantum channel capacity and the hashing bound. We also thank Mackenzie Shaw for pointing out that the square-lattice GKP code admits an induced  $XZ$  2-Pauli noise channel under a symmetric Gaussian random displacement noise model. MS and SF acknowledge financial support from the Intel corporation. AJ is supported by the Einstein Research Unit “Perspectives of a quantum digital transformation”.

*Author Contributions.* — JF developed and implemented the tensor-network decoder during his master thesis, under the supervision of MS and SF. MS wrote the manuscript. AJ, CC, and SF provided project guidance.

- [1] J. Preskill, Reliable quantum computers, Proceedings of the Royal Society of London. Series A: Mathematical, Physical and Engineering Sciences **454**, 385 (1998).
- [2] J. Preskill, Quantum computing in the nisq era and beyond, *Quantum* **2**, 79 (2018).
- [3] J. Preskill, Fault-tolerant quantum computation, in *Introduction to quantum computation and information* (World Scientific, 1998) pp. 213–269.
- [4] D. Gottesman, *Stabilizer codes and quantum error correction* (California Institute of Technology, 1997).
- [5] A. G. Fowler, M. Mariantoni, J. M. Martinis, and A. N. Cleland, Surface codes: Towards practical large-scale quantum computation, *Physical Review A* **86**, 032324 (2012).
- [6] S. Krinner, N. Lacroix, A. Remm, A. Di Paolo, E. Genois, C. Leroux, C. Hellings, S. Lazar, F. Swiadek, J. Herrmann, *et al.*, Realizing repeated quantum error correction in a distance-three surface code, *Nature* **605**, 669 (2022).
- [7] C. Ryan-Anderson, J. G. Bohnet, K. Lee, D. Gresh, A. Hankin, J. Gaebler, D. Francois, A. Chernoguzov, D. Lucchetti, N. C. Brown, *et al.*, Realization of real-time fault-tolerant quantum error correction, *Physical Review X* **11**, 041058 (2021).
- [8] Suppressing quantum errors by scaling a surface code logical qubit, *Nature* **614**, 676 (2023).
- [9] B. M. Terhal, Quantum error correction for quantum memories, *Reviews of Modern Physics* **87**, 307 (2015).
- [10] M. A. Nielsen and I. L. Chuang, *Quantum computation and quantum information* (Cambridge university press, 2010).
- [11] M. M. Wilde, *Quantum information theory* (Cambridge university press, 2013).
- [12] K. Takeda, A. Noiri, T. Nakajima, T. Kobayashi, and S. Tarucha, Quantum error correction with silicon spin qubits, *Nature* **608**, 682 (2022).
- [13] L. Egan, D. M. Debroy, C. Noel, A. Risinger, D. Zhu, D. Biswas, M. Newman, M. Li, K. R. Brown, M. Cetina, *et al.*, Fault-tolerant control of an error-corrected qubit, *Nature* **598**, 281 (2021).
- [14] J. F. Marques, B. Varbanov, M. Moreira, H. Ali, N. Muthusubramanian, C. Zachariadis, F. Battistel, M. Beekman, N. Haider, W. Vlothuizen, *et al.*, Logical-qubit operations in an error-detecting surface code, *Nature Physics* **18**, 80 (2022).
- [15] C. K. Andersen, A. Remm, S. Lazar, S. Krinner, N. Lacroix, G. J. Norris, M. Gabureac, C. Eichler, and A. Wallraff, Repeated quantum error detection in a surface code, *Nature Physics* **16**, 875 (2020).
- [16] D. A. Herrera-Martí, T. Gefen, D. Aharonov, N. Katz, and A. Retzker, Quantum error-correction-enhanced magnetometer overcoming the limit imposed by relaxation, *Phys. Rev. Lett.* **115**, 200501 (2015).
- [17] M. H. Shaw, A. C. Doherty, and A. L. Grimsmo, Logical gates and read-out of superconducting gottesman-kitaev-preskill qubits, arXiv preprint arXiv:2403.02396 (2024).
- [18] L. Hänggli, M. Heinze, and R. König, Enhanced noise resilience of the surface-gottesman-kitaev-preskill code via designed bias, *Physical Review A* **102**, 052408 (2020).
- [19] A. L. Grimsmo and S. Puri, Quantum error correction with the gottesman-kitaev-preskill code, *PRX Quantum* **2**, 020101 (2021).
- [20] D. Gottesman, A. Kitaev, and J. Preskill, Encoding a qubit in an oscillator, *Physical Review A* **64**, 012310 (2001).
- [21] A. Dua, A. Kubica, L. Jiang, S. T. Flammia, and M. J. Gullans, Clifford-deformed surface codes, *PRX Quantum* **5**, 010347 (2024).
- [22] E. Huang, A. Pesah, C. T. Chubb, M. Vasmer, and A. Dua, Tailoring three-dimensional topological codes for biased noise, *PRX Quantum* **4**, 030338 (2023).
- [23] B. Srivastava, A. F. Kockum, and M. Granath, The  $xyz^2$  hexagonal stabilizer code, *Quantum* **6**, 698 (2022).
- [24] D. K. Tuckett, A. S. Darmawan, C. T. Chubb, S. Bravyi, S. D. Bartlett, and S. T. Flammia, Tailoring surface codes for highly biased noise, *Phys. Rev. X* **9**, 041031 (2019).
- [25] Q. Xu, N. Mannucci, A. Seif, A. Kubica, S. T. Flammia, and L. Jiang, Tailored  $zxzx$  codes for biased noise, *Phys. Rev. Res.* **5**, 013035 (2023).
- [26] J. P. Bonilla Ataides, D. K. Tuckett, S. D. Bartlett, S. T. Flammia, and B. J. Brown, The  $zxzx$  surface code, *Nature communications* **12**, 2172 (2021).
- [27] K. Tiurev, A. Pesah, P.-J. H. Derks, J. Roffe, J. Eisert, M. S. Kesselring, and J.-M. Reiner, The domain wall color code, arXiv preprint arXiv:2307.00054 (2023).
- [28] J. Bausch and F. Leditzky, Error thresholds for arbitrary pauli noise, *SIAM Journal on Computing* **50**, 1410 (2021).
- [29] F. Pastawski, B. Yoshida, D. Harlow, and J. Preskill, Holographic quantum error-correcting codes: Toy models for the bulk/boundary correspondence, *Journal of High Energy Physics* **2015**, 1 (2015).
- [30] R. J. Harris, E. Coupe, N. A. McMahon, G. K. Brennen, and T. M. Stace, Decoding holographic codes with an integer optimization decoder, *Physical Review A* **102**, 062417 (2020).
- [31] T. Farrelly, R. J. Harris, N. A. McMahon, and T. M. Stace, Tensor-network codes, *Physical Review Letters* **127**, 040507 (2021).
- [32] R. J. Harris, N. A. McMahon, G. K. Brennen, and T. M. Stace, Calderbank-shor-steane holographic quantum error-correcting codes, *Physical Review A* **98**, 052301 (2018).
- [33] A. Jahn and J. Eisert, Holographic tensor network models and quantum error correction: a topical review, *Quantum Science and Technology* **6**, 033002 (2021).
- [34] T. Farrelly, N. Milicevic, R. J. Harris, N. A. McMahon, and T. M. Stace, Parallel decoding of multiple logical qubits in tensor-network codes, *Phys. Rev. A* **105**, 052446 (2022).
- [35] H. Bombin, R. S. Andrist, M. Ohzeki, H. G. Katzgraber, and M. A. Martin-Delgado, Strong resilience of topological codes to depolarization, *Physical Review X* **2**, 021004 (2012).
- [36] J. Fern and K. B. Whaley, Lower bounds on the nonzero capacity of pauli channels, *Phys. Rev. A* **78**, 062335 (2008).
- [37] D. A. Lidar and T. A. Brun, *Quantum error correction* (Cambridge university press, 2013).
- [38] S. Cree, K. Dolev, V. Calvera, and D. J. Williamson, Fault-tolerant logical gates in holographic stabilizer codes are severely restricted, *PRX Quantum* **2**, 030337 (2021).
- [39] C. Cao and B. Lackey, Approximate bacon-shor code and holography, *Journal of High Energy Physics* **2021**, 1 (2021).
- [40] F. Pastawski and J. Preskill, Code properties from holographic geometries, *Phys. Rev. X* **7**, 021022 (2017).
- [41] C. Cao, J. Pollack, and Y. Wang, Hyperinvariant multiscale entanglement renormalization ansatz: Approximate holographic error correction codes with power-law correlations, *Phys. Rev. D* **105**, 026018 (2022).
- [42] J. Pollack, P. Rall, and A. Rocchetto, Understanding holographic error correction via unique algebras and atomic examples, *Journal of High Energy Physics* **2022**, 1 (2022).
- [43] I. H. Kim and M. J. Kastoryano, Entanglement renormalization,

- quantum error correction, and bulk causality, *Journal of High Energy Physics* **2017**, 1 (2017).
- [44] R. Shen, Y. Wang, and C. Cao, Quantum lego and xp stabilizer codes, arXiv preprint arXiv:2310.19538 (2023).
- [45] E. Witten, Anti-de Sitter space and holography, *Adv. Theor. Math. Phys.* **2**, 253 (1998).
- [46] J. Maldacena, *International Journal of Theoretical Physics* **38**, 1113 (1999).
- [47] S. Gubser, I. Klebanov, and A. Polyakov, Gauge theory correlators from non-critical string theory, *Physics Letters B* **428**, 105 (1998).
- [48] H. N astase, *Introduction to the AdS/CFT Correspondence* (Cambridge University Press, 2015).
- [49] M. Rangamani, T. Takayanagi, M. Rangamani, and T. Takayanagi, *Holographic entanglement entropy* (Springer, 2017).
- [50] A. Almheiri, X. Dong, and D. Harlow, Bulk Locality and Quantum Error Correction in AdS/CFT, *JHEP* **04**, 163, arXiv:1411.7041 [hep-th].
- [51] D. Harlow, TASI Lectures on the Emergence of Bulk Physics in AdS/CFT, *PoS TASI2017*, 002 (2018), arXiv:1802.01040 [hep-th].
- [52] C. Cao and B. Lackey, Quantum lego: Building quantum error correction codes from tensor networks, *PRX Quantum* **3**, 020332 (2022).
- [53] L. Boyle, M. Dickens, and F. Flicker, Conformal quasicrystals and holography, *Phys. Rev. X* **10**, 011009 (2020).
- [54] A. Jahn, Z. Zimbor as, and J. Eisert, Central charges of aperiodic holographic tensor-network models, *Phys. Rev. A* **102**, 042407 (2020).
- [55] M. Steinberg, J. Fan, R. J. Harris, D. Elkouss, S. Feld, and A. Jahn, Far from perfect: Quantum error correction with (hyperinvariant) evenbly codes, arXiv preprint arXiv:2407.11926 (2024).
- [56] N. P. Breuckmann and J. N. Eberhardt, Quantum low-density parity-check codes, *PRX Quantum* **2**, 040101 (2021).
- [57] G. Angl es Munn e, V. Kasper, and F. Huber, Engineering holography with stabilizer graph codes, *npj Quantum Information* **10**, 48 (2024).
- [58] Z. Raissi, A. Burchardt, and E. Barnes, General stabilizer approach for constructing highly entangled graph states, *Phys. Rev. A* **106**, 062424 (2022).
- [59] Z. Raissi, A. Teixid o, C. Gogolin, and A. Ac ın, Constructions of  $k$ -uniform and absolutely maximally entangled states beyond maximum distance codes, *Phys. Rev. Res.* **2**, 033411 (2020).
- [60] W. Helwig, Absolutely maximally entangled qudit graph states, arXiv preprint arXiv:1306.2879 (2013).
- [61] N. Bao, C. Cao, and G. Zhu, Deconfinement and error thresholds in holography, *Phys. Rev. D* **106**, 046009 (2022).
- [62] C. Cao, M. J. Gullans, B. Lackey, and Z. Wang, Quantum Lego Expansion Pack: Enumerators from Tensor Networks, arXiv preprint arXiv:2308.05152 (2023).
- [63] J. Fan, M. Steinberg, A. Jahn, C. Cao, and S. Feld, Heterogeneous concatenation of holographic codes using quantum reed-muller codes, In Preparation (2024).
- [64] T. Jochym-O’Connor and R. Laflamme, Using concatenated quantum codes for universal fault-tolerant quantum gates, *Phys. Rev. Lett.* **112**, 010505 (2014).
- [65] C. Chamberland, T. Jochym-O’Connor, and R. Laflamme, Thresholds for universal concatenated quantum codes, *Phys. Rev. Lett.* **117**, 010501 (2016).
- [66] J. Fan, M. Steinberg, A. Jahn, C. Cao, R. T. Camblor, A. Sarkar, and S. Feld, Holo\_qec: A python package for the design and simulation of holographic quantum error correction codes, In Preparation. (2024).
- [67] S. Bravyi, M. Suchara, and A. Vargo, Efficient algorithms for maximum likelihood decoding in the surface code, *Physical Review A* **90**, 032326 (2014).
- [68] A. Robertson, C. Granade, S. D. Bartlett, and S. T. Flammia, Tailored codes for small quantum memories, *Phys. Rev. Appl.* **8**, 064004 (2017).
- [69] M. Steinberg, S. Feld, and A. Jahn, Holographic codes from hyperinvariant tensor networks, *Nature Communications* **14**, 7314 (2023).
- [70] G. Evenbly, Hyperinvariant tensor networks and holography, *Physical review letters* **119**, 141602 (2017).
- [71] M. Steinberg and J. Prior, Conformal properties of hyperinvariant tensor networks, *Scientific Reports* **12**, 532 (2022).
- [72] S. Bravyi and A. Kitaev, Universal quantum computation with ideal clifford gates and noisy ancillas, *Physical Review A* **71**, 022316 (2005).
- [73] S. Bravyi and J. Haah, Magic-state distillation with low overhead, *Physical Review A* **86**, 052329 (2012).
- [74] N. Bao, C. Cao, and V. P. Su, Magic state distillation from entangled states, *Phys. Rev. A* **105**, 022602 (2022).
- [75] M. A. Webster, B. J. Brown, and S. D. Bartlett, The xp stabiliser formalism: a generalisation of the pauli stabiliser formalism with arbitrary phases, *Quantum* **6**, 815 (2022).
- [76] J. Fan, *Biased-Noise Threshold Studies for Holographic Quantum Error-Correction Codes*, Master’s thesis, QuTech, Technical University of Delft, Delft, the Netherlands (2024).

## Appendix A: Seed Tensors for Other Holographic Codes

The seed tensors and their associated logical operators and their stabilizers are shown in Table II. Here we have used the notation  $\bar{X}X$  to denote  $X \otimes X$  for brevity. Additionally, the final entry for each stabilizer generator (with a bar above) denotes the action on the logical index.

## Appendix B: Threshold Results for Select Data Points

In Figure 5 we display the individual threshold curves obtained for the zero-rate HaPPY code for depolarizing noise, as well as for biased pure  $X$ , pure  $Y$ , and pure  $Z$  noise. Around the fixed points in subfigures (b)-(d), the recovery rate promptly increases, which is due to several reasons: Firstly, the pure 1-Pauli noise capacity can be shown to be 50%, in agreement with known channel-capacity findings [10]. Secondly, as our tensor-network decoder works essentially as a maximum-likelihood decoder, after the  $p = 0.50$  mark, the decoder selects the most-probable error and returns a pure error vector which is used to correct. Therefore, unlike a minimum weight decoder, the tensor network decoder is still able to provide the right correction with high probability even when  $p > 0.50$ . More details can be found in [30, 76].

Seed Tensor	Stabilizers	Logical Operators
HaPPY	$XZZXI\bar{I}, IXZZX\bar{I}, XIXZZ\bar{I}, ZXIXZ\bar{I}$	$ZZZZZ\bar{Z}, XXXXX\bar{X}$
Steane	$XXIII\bar{X}\bar{I}, IXXXI\bar{X}\bar{I}, III\bar{X}\bar{X}\bar{X}\bar{I}, ZZIII\bar{Z}\bar{I}, IZZZII\bar{Z}\bar{I}, III\bar{Z}\bar{Z}\bar{Z}\bar{I}$	$ZZZZZZ\bar{Z}, XXXXXX\bar{X}$
[[6, 1, 3]]	$ZIZIII\bar{I}, XZYYXI\bar{I}, XXXXZI\bar{I}, IZZXIX\bar{I}, XYXYIZ\bar{I}$	$XZXZII\bar{X}, XYYXII\bar{Z}$
SCF	$XXIXI\bar{I}, IIXXX\bar{I}, ZIZZI\bar{I}, IZIZZ\bar{I}$	$XIXII\bar{X}, IIZIZ\bar{Z}$

TABLE II. Seed tensors and their stabilizers, as well as logical operators for select holographic codes.

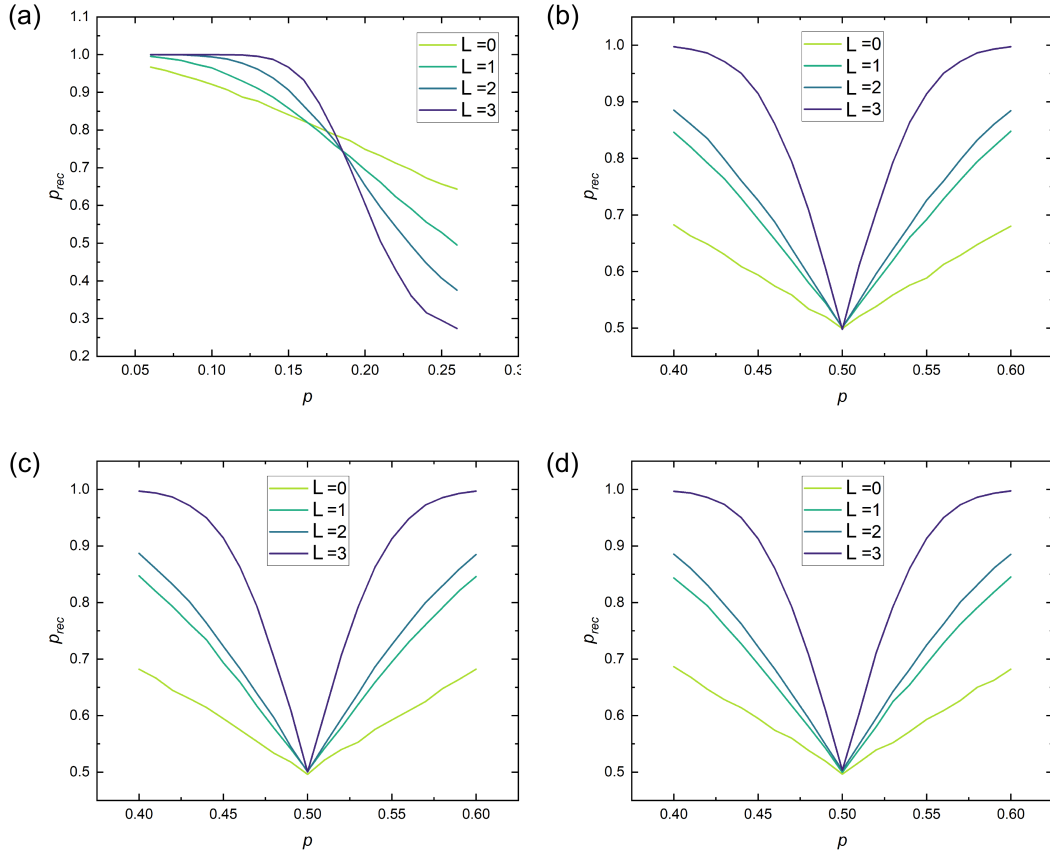


FIG. 5. Threshold curves for depolarizing, pure  $X$ ,  $Y$ , and  $Z$  noise, as studied using the tensor-network decoder, for the zero-rate HaPPY code at up to  $L = 3$  layers of edge inflation.